

# The Fraction of Quiescent Massive Galaxies in the Early Universe

A. Fontana<sup>1</sup>, P. Santini<sup>1,2</sup>, A. Grazian<sup>1</sup>, L. Pentericci<sup>1</sup>, F. Fiore<sup>1</sup>, M. Castellano<sup>1</sup>, E. Giallongo<sup>1</sup>, N. Menci<sup>1</sup>, S. Salimbeni<sup>1,3</sup>, S. Cristiani<sup>4</sup>, M. Nonino<sup>4</sup>, and E. Vanzella<sup>4</sup>

<sup>1</sup> INAF - Osservatorio Astronomico di Roma, Via Frascati 33, 00040 Monteporzio (RM), Italy

<sup>2</sup> Dipartimento di Fisica, Università di Roma “La Sapienza”, P.le A. Moro 2, 00185 Roma, Italy

<sup>3</sup> Department of Astronomy, University of Massachusetts, 710 North Pleasant Street, Amherst, MA 01003

<sup>4</sup> INAF - Osservatorio Astronomico di Trieste, Via G.B. Tiepolo 11, 34131 Trieste, Italy

Received .... ; accepted ....

## ABSTRACT

**Aims.** The aim of this work is to collect a complete, mass-selected sample of galaxies with very low specific star formation rate, for a comparison with the prediction of recent theoretical models.

**Methods.** We use the  $f(24\mu\text{m})/f(K)$  flux ratio, complemented by the SED fitting to the full  $0.35 - 8.0\mu\text{m}$  spectral distribution, to select quiescent galaxies from  $z \simeq 0.4$  to  $z \simeq 4$  in the GOODS-MUSIC sample. Our observational selection can be translated into thresholds on the specific star formation rate  $\dot{M}/M_*$ , that can be used to compare with the theoretical predictions.

**Results.** We find that, in the framework of the well known global decline of the quiescent fraction with redshift, a non-negligible fraction  $\simeq 15 - 20\%$  of massive galaxies with very low specific star formation rate exists up to  $z \simeq 4$ , including a tail of “Red&Dead” galaxies with  $\dot{M}/M_* < 10^{-11}\text{yr}^{-1}$ . Recent theoretical models vary to a large extent in the prediction of the fraction of galaxies with very low specific star formation rates, and are unable to provide a global match to our data.

**Conclusions.**

**Key words.** Galaxies:distances and redshift - Galaxies: evolution - Galaxies: high redshift

## 1. Introduction

Understanding the process of formation and evolution of early type galaxies is a major goal of present-day cosmology, as well as a fundamental benchmark for “ab-initio” theoretical models of galaxy evolution.

According to several independent lines of evidence, the population of massive galaxies has undergone a major evolution during the epoch corresponding to the redshift range  $1.5 - 3$ , where the galaxy stellar mass function shows a strong evolution at high masses (Berta et al. 2007; Fontana et al. 2006) (F06 in the following), massive galaxies settle on the Hubble sequence (e.g. Abraham et al. 2007; Franceschini et al. 2006) and the red sequence appears in high  $z$  clusters (e.g. Zirm et al. 2008).

The nature of the physical processes that led to this rapid rise remains largely unexplored. A large number of massive ( $\simeq 10^{11} M_\odot$ ) actively star-forming galaxies is clearly in place at  $z \simeq 2$  (Daddi et al. 2004; Papovich et al. 2007), with a trend of more massive galaxies to be the more actively star-forming (Daddi et al. 2007b), at variance with the local Universe.

At the same time, the existence of galaxies with low levels of star formation rates at  $z \simeq 1.5 - 2$  has been indicated by imaging surveys based on color criteria (e.g. Daddi et al. 2004) or SED fitting (Grazian et al. 2007), and by spectroscopic observations of red galaxy samples (Cimatti et al. 2004; Saracco et al. 2005; Kriek et al. 2006). These results have motivated the inclusion of efficient methods for providing a fast assembling of massive galaxies at high  $z$  (such as starburst during interactions) as well as quenching of the SFR, most notably via AGN feedback (Menci et al. 2006; Bower et al. 2006; Hopkins et al. 2008).

Unfortunately, a detailed validation of the prediction of theoretical models has been hampered so far by the lack of a statistically well defined sample of early type galaxies at high redshift, and by the difficulty in defining a common criterium to identify such early type galaxies in the data. It is indeed difficult to isolate passively evolving galaxies from the wider population of intrinsically red galaxies at high redshift, which include also a (probably larger) contribution of dust enshrouded star-forming galaxies. The two classes are indeed indistinguishable when selected by means of a single color criterium, such as the “ERO” classification ( $R - K > 4$ ) (Daddi et al. 2000; McCarthy 2004) or the “DRG” one ( $J - K > 2$ ) (Franx et al. 2003; van Dokkum et al. 2003). The corresponding SEDs, however, are not degenerate and can be distinguished with more complex criteria, even when spectroscopy is not feasible. Some of such criteria adopt more colors, like the  $I - J/J - K$  method proposed by Pozzetti & Mannucci (2000), and spectroscopically confirmed by Cimatti et al. (2003), or the  $B_zK$  method proposed by Daddi et al. (2004). Other methods rely on the spectral fitting of the overall SED, either making use of the resulting rest-frame colors, as in the case of the  $U - V/V - I$  criteria proposed by Wuyts et al. (2007), or directly using the output of the SED fitting process (Arnouts et al. 2007; Salimbeni et al. 2008; Grazian et al. 2007).

We already used the latter method in our recent analysis of the GOODS-S data set, to disentangle the different contributors to the mass density at high redshift (Grazian et al. 2007) and to describe the evolution of the luminosity function of red galaxies up to  $z \simeq 3$  (Salimbeni et al. 2008).

In this work, we shall use the additional information available thanks to observations in the mid-IR  $24\mu\text{m}$  band, to allow a more careful selection of high redshift passively evolving galaxies.

Send offprint requests to: A. Fontana, e-mail: fontana@oa-roma.inaf.it

ies, with the specific aim of comparing their number density with the theoretical expectations.

We shall use a revised version of our GOODS-MUSIC sample (Grazian et al. 2006), a 15 bands multicolor (U-to- $24\mu\text{m}$ ) catalog extracted from the 143.2 sq. arcmin. area of the GOODS-South public survey. The key improvements with respect to our previous works are a revised IRAC photometry and the addition of the  $24\mu\text{m}$  flux for all objects in the catalog. Full details are given in a companion paper (Santini et al. 2009, S09 in the following). Another important difference is that we have included all the objects detected in the  $4.5\mu\text{m}$  image, down to  $m_{45} < 23.5$ . In the following, we will adopt a mass-selected sample, obtained cutting at  $M_* \geq 7 \times 10^{10} M_\odot$  our photometric catalog based on a combined selection  $K < 23.5$  or  $m_{45} < 23.5$ . This photometric sample is complete at this mass limit up to  $z \simeq 4$ , including also extinguished galaxies (see F06).

Observed and rest-frame magnitudes are in the AB system, and we adopt the  $\Lambda$ -CDM concordance model ( $H_0 = 70 \text{ km/s/Mpc}$ ,  $\Omega_M = 0.3$  and  $\Omega_\Lambda = 0.7$ ).

## 2. Quiescent galaxies

### 2.1. The role of Mid-IR observations

In principle, the observed mid-IR flux is a powerful tool to distinguish the two classes of red galaxies at high redshift. Dust-absorbed star-forming galaxies are expected to be bright in the mid-IR, where most of the UV light absorbed by dust is irradiated. On the contrary, passively evolving galaxies, are expected to be much dimmer, since ordinary stars have low emission at IR wavelengths. To quantify this criterium, we use the ratio  $f(24\mu\text{m})/f(K)$  between the observed flux at  $24\mu\text{m}$  and the  $K$  band one. We show the  $f(24\mu\text{m})/f(K)$  for all galaxies in our sample in Fig.1, in four redshift bins. To show how this color can differentiate between galaxy types, we have computed the same  $f(24\mu\text{m})/f(K)$  up to  $z \simeq 4$  using a set of local templates which includes early type, spiral and starburst galaxies (Polletta et al. 2007). All templates have been  $k$ -corrected at the different redshifts. As shown in Fig.1, the loci populated by the different galaxy types in the  $U - V$  vs  $f(24\mu\text{m})/f(K)$  plane are well distinguished and allow a fair distinction between very actively star-forming galaxies and those with moderate-to-low star formation.

In Fig.1 we show the observed  $f(24\mu\text{m})/f(K)$  for the complete  $M_* \geq 7 \times 10^{10} M_\odot$  sample, both for individual galaxies as well as its distribution. Upper limits derive from  $1\sigma$  upper limits in the  $24\mu\text{m}$  photometry. It is clearly shown in Fig.1 that the  $f(24\mu\text{m})/f(K)$  ratio of star-forming galaxies increases with redshift, and that a numerous population of starburst appears at  $z > 1$ , with colors similar to local, rarer, LIRGs. On the other side few bright galaxies at low and intermediate redshift, with low star formation rates are still detected at very low levels in the  $24\mu\text{m}$  image.

The most striking result is that the distribution of the  $f(24\mu\text{m})/f(K)$  is clearly bimodal, with a minimum in correspondence of the gap between the loci of active and passive galaxies. The observed minima in the distribution of the  $f(24\mu\text{m})/f(K)$  ratio occurs at  $f(24\mu\text{m})/f(K) = 1, 2, 5, 6$  in the four redshift bins adopted in Fig.1. Two warnings are needed about this bimodality. First, it is somewhat emphasized by the upper limits at faint  $24\mu\text{m}$  levels, the true distribution being likely more spread at even lower  $f(24\mu\text{m})/f(K)$ . More important, the bimodality would disappear if a deeper catalog would be used (for instance, the  $z \leq 26$  selected version of

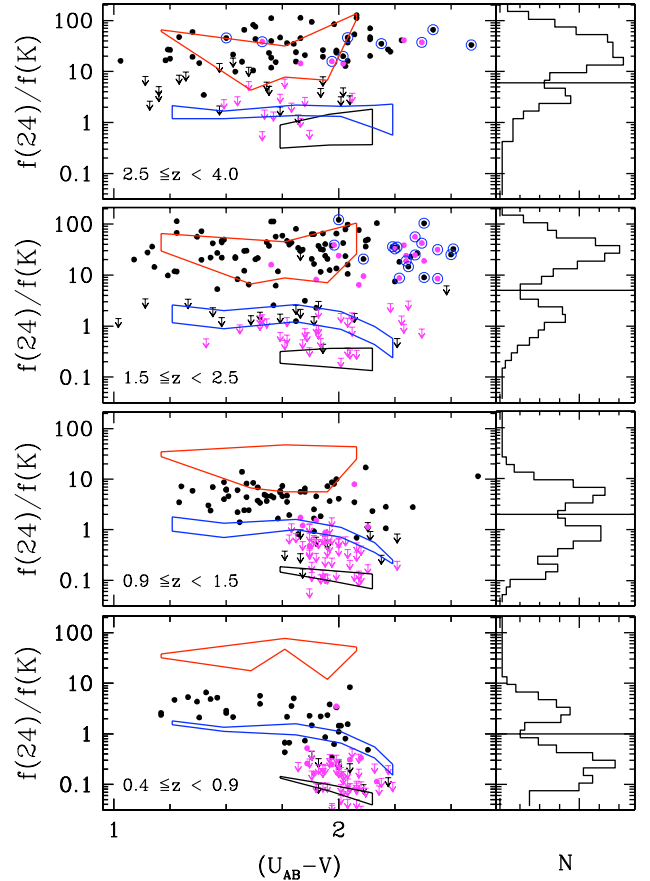


**Fig. 1.** Ratio between the observed fluxes at  $24\mu\text{m}$  and in the  $K$  band as a function of the rest-frame  $U - V$  color, in four redshift bins, for the  $M_* \geq 7 \times 10^{10} M_\odot$  sample. Upper limits correspond to objects fainter than  $20\mu\text{Jy}$  in the  $24\mu\text{m}$  image. Galaxies fit with  $\text{age}/\tau > 6$  (as discussed in Section 3) are shown in magenta. Large blue circles are the “obscured AGN” candidates of Fiore et al. (2008). Closed areas represent the range of  $f(24\mu\text{m})/f(K)$  obtained by redshifting a set of local samples (Polletta et al. 2007): from bottom to top, early type galaxies (black line), spirals (blue line), starbursts (red line).

GOODS-MUSIC catalog). The high mass-limit of our sample, indeed, preferentially select very red galaxies, as shown by their large  $U - V$  color, which are those where the bimodality is clearly detected. This is a key feature of our approach, since the  $f(24\mu\text{m})/f(K)$  ratio provides a natural way to distinguish between active and quiescent galaxies within the population of high redshift, red galaxies.

### 2.2. The selection on rest-frame quantities

The criterium that we adopted to identify quiescent galaxies cannot be directly applied to the output of current theoretical models for galaxy formation and evolution, that typically do not predict the mid-IR flux. The comparison is instead natural if we convert the data into the quantities immediately provided by these models, i.e. stellar mass or star formation rates. We will use the stellar masses  $M_*$  provided by the SED fitting, with accuracy

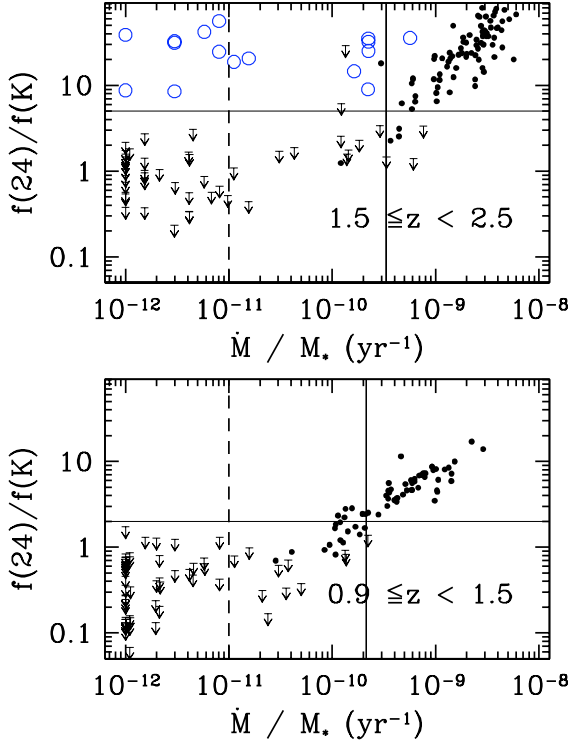


**Fig. 2.** Ratio between the observed fluxes at  $24\mu\text{m}$  and in the  $K$  band as a function of the Specific Star Formation Rate ( $\dot{M}/M_*$ ), for the sample with  $M_* \geq 7 \times 10^{10} M_\odot$ . Galaxies with  $\dot{M}/M_* < 10^{-12} \text{ yr}^{-1}$  have been arbitrarily set to  $\dot{M}/M_* = 10^{-12} \text{ yr}^{-1}$ . Upper limits refer to objects fainter than  $20\mu\text{Jy}$  in the  $24\mu\text{m}$  image. Large blue circles are the “obscured AGN” candidates of Fiore et al. (2008). The solid vertical line corresponds to the inverse of the age of the Universe at the centre of the redshift bin. The dashed vertical line shows the threshold on  $\dot{M}/M_*$  adopted to classify “Red&Dead” galaxies. The horizontal solid line refers to the minimum in the observed distribution of the  $f(24\mu\text{m})/f(K)$  ratio in the same redshift range.

described at length in F06, and briefly in Sect.3. To obtain star formation rates for galaxies detected at  $24\mu\text{m}$ , we use the recipe of Papovich et al. (2007) to convert the  $24\mu\text{m}$  + rest-frame UV luminosity into a total star formation rate, using the Dale & Helou (2002) models with a (lowering) correction at large mid-IR fluxes. For galaxies below  $20\mu\text{Jy}$  at  $24\mu\text{m}$ , we use the SFR derived from the SED fitting. As we show in S09 (see also Daddi et al. 2007b), these two SFR estimators agree relatively well, especially at low SFR levels.

In Fig.2 we show the correlation between the  $f(24\mu\text{m})/f(K)$  ratio and  $\dot{M}/M_*$  in our sample. For simplicity, we plot only the two redshift range which are more populated in our sample: the same trend holds at higher and lower redshifts. To some extent, this correlation is largely expected given the relationship between  $\dot{M}$  and the  $24\mu\text{m}$  flux on the one side, and  $M_*$  and the  $K$  magnitude on the other. The key point, however, is that the correlation is so narrow that it allows to translate the (observational) criterium based on the  $f(24\mu\text{m})/f(K)$  ratio (horizontal line in Fig.2) into a (model-oriented) cut on the estimated  $\dot{M}/M_*$  (vertical line in Fig.2). As shown in Fig.2, the two samples in practice coincide.

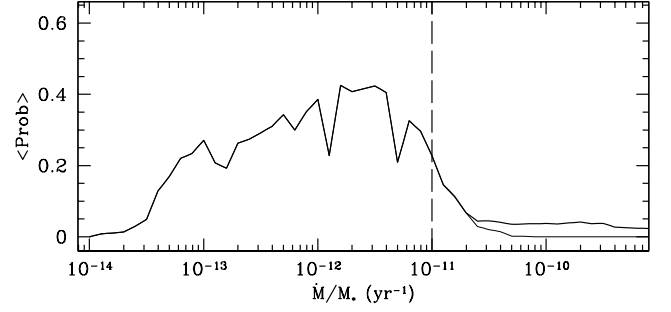


**Fig. 3.** Probability distribution of the  $\dot{M}/M_*$  ratio in the sample of “Red&Dead” galaxies at  $1.5 \leq z \leq 2.5$ , averaged over the whole sample. The thick curve shows the probability distribution of the SED fitting to the 14 bands SED, from the U band to the  $8\mu\text{m}$  band. The thin curve shows the probability distribution removing models that over predict the SFR with respect to the upper limit provided by the constraint at  $24\mu\text{m}$ . The dashed vertical line shows the limit  $\dot{M}/M_* < 10^{-11} \text{ yr}^{-1}$  that we adopt to define “Red&Dead” galaxies.

Based on this evidence, we shall use the Specific Star Formation Rate  $\dot{M}/M_*$  to select quiescent galaxies, allowing a clean comparison with the theoretical models. Given that  $\dot{M}/M_*$  is dimensionally the inverse of a timescale, a natural threshold on  $\dot{M}/M_*$  is the inverse of the age of the Universe at the corresponding redshift  $(t_U(z))^{-1}$ . We will define galaxies with  $\dot{M}/M_* < (t_U(z))^{-1}$  as “Quiescent” in the following. Such a name is motivated by the fact that - by definition - these galaxies have experienced a major episode of star formation prior to the observations<sup>1</sup>.

### 3. “Red&Dead” Galaxies

#### 3.1. Basic definitions

Galaxies defined as “Quiescent” with the criterium shown in the previous section may still have a measurable amount of ongoing SFR (e.g.  $\dot{M} \simeq 10 M_\odot/\text{yr}$  for a  $M_* \simeq 10^{11} M_\odot$  galaxy). It is therefore interesting to estimate the fraction of galaxies with very low or negligible levels of SFR. As we will show in the following, these objects, that we label “Red&Dead”, constitute a sterner test to theoretical models.

To select galaxies at high redshift on the basis of very low star formation rates we need to complement the results based on the  $f(24\mu\text{m})/f(K)$  ratio with the outputs of the fitting analysis to the optical-IR observed SED. The lack of detection in the  $24\mu\text{m}$  image provides indeed only an upper limit on the ongoing SFR (see for instance Fig.2), and its exact level can be estimated from the SED fitting only. We have applied the SED fitting technique following the recipe described in several papers (see Fontana et al. (2004) and F06 for details). The U-to- $8\mu\text{m}$  photometry has been compared with a grid of models drawn from the Bruzual&Charlot spectral synthesis code, characterized by exponentially declining star formation histories with timescale  $\tau$  and a set of ages, metallicities and dust extinction. For comparison with our previous works, and with most of the literature, we use the standard Salpeter IMF and the BC03 models. We have

<sup>1</sup> Indeed, if  $M_* = \langle \dot{M} \rangle_{\text{past}} \times t_U(z)$ , where  $\langle \dot{M} \rangle_{\text{past}}$  is the star formation rate averaged over the whole age of the Universe at the corresponding  $z$ , the requirement  $\dot{M}/M_* < (t_U(z))^{-1}$  implies  $\dot{M} \leq \langle \dot{M} \rangle_{\text{past}}$ .

however verified that the adoption of the most recent version of the code incorporating the treatment of the post-AGB stars (Bruzual A 2007) does not change our results significantly (see Salimbeni et al. 2009 for a preliminary analysis). In particular, only 1 (out of 144) objects classified as “Red&Dead” would not be classified as such with the new version.

To select “Red&Dead” galaxies, we will use a constant, strict threshold  $\dot{M}/M_* < 10^{-11} \text{yr}^{-1}$  (vertical dashed line in Fig.2). To some extent, such a threshold is arbitrary, the important point being that we shall adopt the very same cut on theoretical models, to ensure a proper comparison. However, we note that the same threshold has also been used previously (Brinchmann et al. 2004) to separate active and quiescent galaxies.

It is interesting to note that it also corresponds to a threshold  $\text{age}/\tau > 6$  between the fitted age and the star formation exponential timescale  $\tau$ . This follows from the fact that, assuming exponentially declining star formation histories, the specific star formation rate can be computed analytically and is  $\dot{M}/M_* = (\tau(e^{\text{age}/\tau} - 1))^{-1}$ , yielding  $\dot{M}/M_* \approx 10^{-11} \text{yr}^{-1}$  for  $\text{age}/\tau \approx 6$ , for small values of  $\tau$ . This coincidence allows us to compare the pure SED fitting approach with the additional analysis provided by the  $24\mu\text{m}$  data. Indeed, a threshold on  $\text{age}/\tau$  has already been applied (Arnouts et al. 2007; Salimbeni et al. 2008; Grazian et al. 2007) to broadly identify passively evolving galaxies, although with a less conservative value  $\text{age}/\tau > 4$ . At this purpose, we plot in Fig.1 the location in the  $U - V$  vs.  $f(24\mu\text{m})/f(K)$  plane of all galaxies with  $\text{age}/\tau > 6$  (magenta points). It is shown that the classification scheme based purely on the optical–near IR SED fitting agrees very well with the  $f(24\mu\text{m})/f(K)$  criterium, providing an important consistency check. The main notable exception are a number of “Compton thick AGN” candidates at  $1.5 < z < 2.5$ , selected as in Fiore et al. (2008), where the  $24\mu\text{m}$  emission is ascribed to an AGN activity. These objects will be further discussed in Sect. 3.4.

We remark that we select “Red&Dead” galaxies by requiring  $\dot{M}/M_* < 10^{-11} \text{yr}^{-1}$ , not simply  $\text{age}/\tau > 6$ . The difference is due to how we estimate SFR: we assign the SED–derived ones only to objects essentially undetected in the mid-IR, i.e. those with  $24\mu\text{m}$  flux below  $20\mu\text{Jy}$ . For this reason, the few objects fitted with  $\text{age}/\tau > 6$  but with large  $f(24\mu\text{m})/f(K)$  are not included in our sample of “Red&Dead” galaxies. In the rest of this section we will discuss the accuracy of this method for the most interesting subsample, i.e. for “Red&Dead” galaxies at  $z \geq 1.5$ .

### 3.2. “Red&Dead” Galaxies at $1.5 \leq z \leq 2.5$

A sizeable fraction of the sample with  $\dot{M}/M_* < 10^{-11} \text{yr}^{-1}$  lies in the redshift range  $1.5 \leq z \leq 2.5$ , where we detect 32 galaxies. The reliability of their  $\dot{M}/M_*$  measure can be assessed using the error analysis that has already been widely adopted in similar cases (Papovich et al. 2001, F06). Briefly, the full synthetic library used to find the best-fitting spectrum is compared with the observed SED of each galaxy. For each spectral model (i.e. for each combination of the free parameters  $\text{age}$ ,  $\tau$ ,  $Z$ ,  $E(B - V)$ ) the probability  $P$  of the resulting  $\chi^2$  is computed and retained, along with the associated  $\dot{M}$  and  $M_*$ . The ensemble of  $\dot{M}/M_*$  values corresponding to probabilities above a given minimum threshold defines the range of acceptable values for  $\dot{M}/M_*$ . Since most of our “Red&Dead” galaxies have only a photometric redshift, for such objects we have computed this analysis leaving the redshift free. We show in Fig.3 the resulting distribution of the probability  $P$ , averaged over the whole sample of “Red&Dead” galaxies at  $1.5 \leq z \leq 2.5$ . The tail at large values of  $\dot{M}/M_*$  is due to 2 objects with a nearly equal probability of being fitted by a dusty

starburst solution. The large values of  $\dot{M}$  implied would easily over predict the observed flux (actually an upper limit) at  $24\mu\text{m}$ . Taking into account this additional constraint, we also display in Fig.3 the distribution of  $P$  after removing the models that over predict the SFR with respect to the upper limit provided at  $24\mu\text{m}$ . It is clear from Fig.3 that the SED fitting for these galaxies is well constrained at levels  $\dot{M}/M_* < 10^{-11} \text{yr}^{-1}$ , since the probability of having  $\dot{M}/M_*$  has only a small tail above  $10^{-11} \text{yr}^{-1}$ .

This result is not surprising. Since the galaxies in our sample are by selection massive ( $M_* \geq 7 \times 10^{10} M_\odot$ ), the threshold  $\dot{M}/M_* = 10^{-11} \text{yr}^{-1}$  is equivalent in practice to small but still measurable amount of SFR, of the order of  $\approx 1 M_\odot \text{yr}^{-1}$ . Such levels correspond to detectable fluxes in the very deep B-z optical images of GOODS (the magnitude computed from a galaxy with  $\approx 1 M_\odot \text{yr}^{-1}$ , for small values of  $E(B - V)$ , is in the range 26-28 mags) and can then be measured by the full SED fitting.

Another cross check can be done on the small subset of our “Red&Dead” sample which have spectroscopic observations in this redshift range. Using both the K20 and the public GOODS data set, we find 6 objects with spectroscopic redshift. Four of these objects are classified as early spectral type, with no detected OII. Two other objects have both absorption features, typical of evolved systems, as well as a weak OII line. A weak OII line is not necessarily an indicator of ongoing star formation rate (Yan et al. 2006). In any case, adopting the standard conversion of Kennicutt (1998) we derive star formation rates of the order of  $2-3 M_\odot \text{yr}^{-1}$ , consistent with the SED fitting estimates, confirming that these objects have  $\dot{M}/M_* \lesssim 10^{-11} \text{yr}^{-1}$ . We conclude that our analysis is sufficiently solid at  $1.5 < z < 2.5$ , and allows to build a mass selected sample of “Red&Dead” galaxies.

### 3.3. “Red&Dead” Galaxies at $z > 2.5$

As we move to higher redshifts,  $2.5 \leq z \leq 4$ , the analysis becomes more uncertain. First, the constraints based on the  $24\mu\text{m}$  emission become looser or even useless, since this band does not encompass any more the range dominated by dust emission. In addition, objects become even fainter and redder, and they completely lack any spectroscopic confirmation. In this redshift range we detect 12 “Red&Dead” candidates, 9 of which located at  $2.5 < z_{\text{phot}} < 3$ . We have carefully examined each object to assess its reliability. First, we have verified that the photometry is not contaminated by nearby companions, and that the overall SED is smooth and not obviously biased by photometric fakes. All the galaxies selected in this range are very red, with  $z - B > 4$ , making them redder than the typical EROs at lower redshifts. Their optical–IR SED is dominated by a break between the  $K$  and the IRAC bands, with a change of slope that is a signature of evolved galaxy population (star-forming, dusty objects have indeed a more featureless slope). The redshift probability distribution is somewhat broad, typically constraining  $z_{\text{phot}} > 1.5 - 2$  but with a relatively large  $\Delta z_{\text{phot}} \approx 0.5$ .

Quantitatively, the error analysis described above shows that 5 out of the 9 objects at  $2.5 < z_{\text{phot}} < 3$  are well constrained at  $\dot{M}/M_* < 10^{-11} \text{yr}^{-1}$ , even with the broad redshift range allowed. An example of such objects is shown in the upper panel of Fig.4. The four other objects have a wider distribution of the  $\dot{M}/M_*$  (Fig.4, middle panel), as well as in redshift.

In a similar way, the three objects detected at  $z > 3$  are also loosely constrained. They have a clear minimum in the  $\chi^2$  distribution around  $z_{\text{phot}} \approx 3.5 - 4$ , but they still have a tail down to  $z \approx 2$ . The distribution of the acceptable  $\dot{M}/M_*$  also extends significantly beyond  $10^{-11} \text{yr}^{-1}$ .

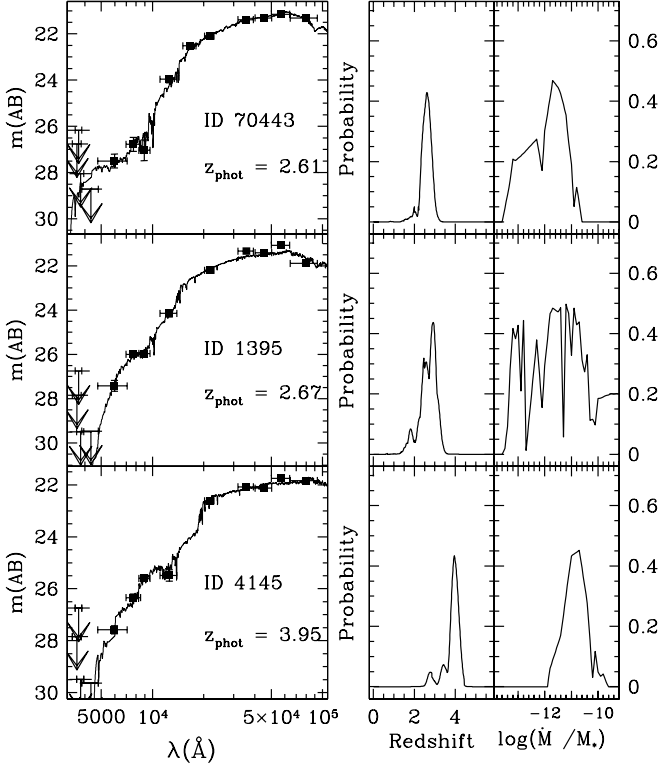


**Fig. 4.** Examples of “Red&Dead” galaxies at  $z > 2.5$ . For each object, from left to right: the observed flux in the GOODS band and the best-fit SED; the redshift probability function; the  $\dot{M}/M_*$  probability distribution. From top to bottom, the three galaxies shown represents three different categories: a robust candidate at  $2.5 < z < 3$ ; a less secure candidate in the same redshift range; a typical example of the candidates at  $z > 3$ .

On the basis of this analysis, we conclude that at least 55% of the our “Red&Dead” candidates at  $2.5 < z_{\text{phot}} < 3$  are robust candidates, while the remaining 45% and the three candidates at  $z > 3$  are more uncertain. It would be natural to convert this finding into an upper limit of the actual number density of “Red&Dead” galaxies. However, we note that a comparable number of galaxies in our sample are classified with  $\dot{M}/M_*$  slightly above  $10^{-11} \text{ yr}^{-1}$ , such that they are not included in our sample, and nevertheless have a range of acceptable models that extends well below  $\dot{M}/M_* = 10^{-11} \text{ yr}^{-1}$ . We conclude that at  $z > 2.5$  the estimate of  $\dot{M}/M_*$  becomes very noisy, mostly due to the limitations provided by the current depth of the existing observations, and that the resulting statistics of “Red&Dead” galaxies is to be treated with more caution. As we shall show in next section, the statistical error (including both Poisson and cosmic variance components) is so large for these small samples that a more rigorous treatment of these uncertainties is likely not necessary.

### 3.4. Hosts of Compton thick AGNs

A potential source of uncertainties in many statistics concerning high redshift galaxies is the contamination due to AGNs. As we

describe in more detail in S09, we have removed from our catalog both the spectroscopically confirmed AGNs and the X-ray sources with an optically dominant point like source. In addition, we have identified the galaxies that likely harbour Compton thick AGNs using the criterium defined in Fiore et al. (2008), which is based on the detection of a mid-IR excess in very red galaxies. This criterium is similar to the one adopted by Daddi et al. (2007a) but includes also objects that are much redder in the optical-IR range than the BzK selected by Daddi et al. (2007a). A full discussion of the SED of these objects will be presented elsewhere: for the moment, we note that 9 of these “Compton thick AGN” candidates at  $1.5 < z < 2.5$  are classified as “Red&Dead” galaxies, as shown in Fig. 1. Unfortunately, the nature of these objects remains quite elusive. Most of these objects are among the reddest in our sample, as indicated by their extreme rest-frame  $U - V$ . They are extremely faint or even undetected in the deep  $z$ -band ACS images, and are included in our sample only thanks to the detection in the  $K$  or in the  $4.5 \mu\text{m}$  image. As a result, the probability distributions of their photometric redshift are often broad, although they are typically constrained to be at  $z_{\text{phot}} > 2$ . Only three (out of nine) galaxies have the distribution of  $\dot{M}/M_*$  constrained to be below  $10^{-11} \text{ yr}^{-1}$ . In the following, we shall not rely on this classification, and we shall therefore compute the fraction of “Red&Dead” galaxies at  $1.5 < z < 2.5$  in three different ways (named *a*), *b*), *c*) in the caption of Fig. 5), in order to explore all possible cases. First, (option *a*)) we shall remove all the “Compton thick AGN” candidates from our sample, irrespective of their SED classification. Alternatively, (option *b*)) we shall assume that none of them is a “Red&Dead” galaxy, in practice providing a lower limit to their fraction. Finally (option *c*)) we shall include them in the statistics, assigning their formal SED classification. As we show in the following section, the fraction computed with these different assumptions changes by  $\approx 20\%$  of its value, still providing interesting constraint on the theoretical models.

## 4. Results and discussion

We can finally compute the fraction of “Quiescent” and “Red&Dead” galaxies in different redshift ranges, following the definitions provided in the last two sections. Such fractions are shown in Fig. 5 as a function of redshift. The different values for “Red&Dead” at  $1.5 < z < 2.5$  reflect the different accounting of the hosts of Compton thick AGNs. Error bars have been computed by summing (in quadrature) the Poisson error and the cosmic variance one. The latter has been computed by measuring the relative variance within 200 samples bootstrapped from the Millennium Simulation (Kitzbichler & White 2007), using an area as large as GOODS-S and applying the same selection criteria.

We remind that we compute such fractions with respect to the total number of galaxies with  $M_* \geq 7 \times 10^{10} M_\odot$  in our sample. Since we are interested in the ratio between galaxy classes, the impact of the exact choice of this threshold is measurable but not dramatic. We have verified that increasing/decreasing the mass limit cut by a factor of 2, the fraction of both “Quiescent” and “Red&Dead” galaxies in different redshift ranges changes by about 0.1, in the data (where applicable) as well as in the theoretical models. A factor of 2 may result by adopting a different IMF, and is of the order of the uncertainty of the stellar mass estimate.

Our analysis confirms the cosmological decrease of massive early type galaxies at large redshifts: quiescent galaxies dominate the population of massive galaxies at  $z \ll 1$ , and become



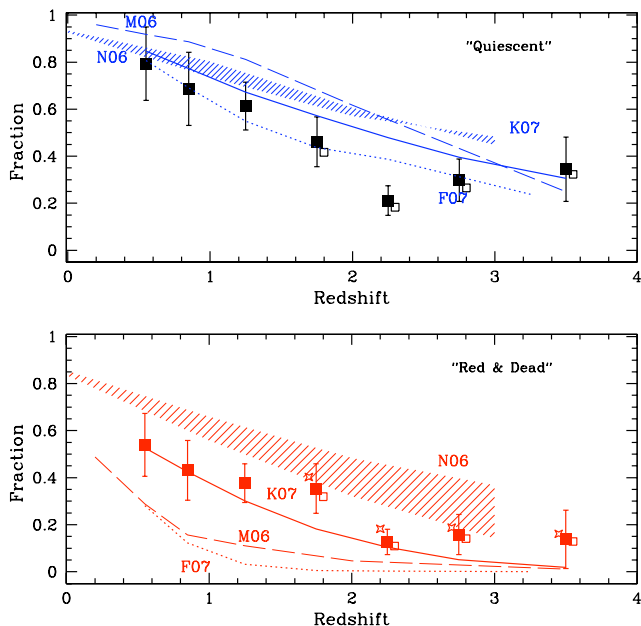


**Fig. 5.** *Lower* Fraction of “Red&Dead” galaxies (defined by  $\dot{M}/M_* < 10^{-11} \text{ yr}^{-1}$ ) as a function of redshift, in the  $M_* \geq 7 \times 10^{10} M_\odot$  mass-selected sample. Points represent the observed values. Filled, open and starred points (slightly offset for clarity) refer to the three different strategies *a, b, c* discussed in the text to account for obscured AGNs. Error bars include Poisson and cosmic variance errors. Lines refer to the predictions of theoretical models, as described by the legend: Menci et al. (2006) (M06), Fontanot et al. (2007) (F07), Kitzbichler & White (2007) (K07), Nagamine et al. (2006), (N06); *Upper* Fraction of “Quiescent” galaxies as a function of redshift, defined by  $\dot{M}/M_* < (t_U(z))^{-1}$ , in the same mass-selected sample. Points and lines as in the lower panel.

progressively less common at higher  $z$ . However, it is important to remark that a significant fraction of galaxies with very low levels of SFR is in place even at the highest redshifts sampled here ( $z \approx 3.5$ ) with a fraction of about 10-15% at  $z > 2$ .

By definition, “Quiescent” massive galaxies have assembled most of their stellar mass in previous epochs, implying that they have either undergone an active starburst phase or important merging process at larger redshifts. The large fraction of “Quiescent” galaxies that we observe at  $z \approx 2$  implies that such processes must have been frequent at very high redshifts. The upper panel of Fig.5 can also be interpreted in terms of “Active” galaxies, i.e. of the complementary fraction with  $\dot{M}/M_* \geq (t_U(z))^{-1}$ . According to the duty-cycle argument presented in S09, such actively star forming galaxies are experiencing a major episode of star formation, potentially building up a substantial fraction of their stellar mass in this episode. Their fraction increases with redshift, making more than 50% of the population of massive galaxies at  $z \geq 2$ .

Finally, the sizeable number of “Red&Dead” galaxies is already in place at  $z > 1.5$ , implying that the star formation episodes must be quenched either by efficient feedback mechanism and/or by the stochastic nature of the hierarchical merging process.

It is interesting to see whether theoretical models agree with these observational evidences. In Fig.5 we plot the prediction

of several such models, applying the same criteria based on the  $\dot{M}/M_*$  values. We consider purely semi-analytical models (Menci et al. (2006), M06, Fontanot et al. (2007), F07), semi-analytical rendition of the Millennium N-body dark matter simulation (Kitzbichler & White (2007), K07), and purely hydrodynamical simulations (Nagamine et al. (2006), N06). The latter are computed with three different timescales  $\tau$  for the star formation rate (ranging from  $2 \times 10^7$  yrs to  $2 \times 10^8$  yrs), and represented with a shaded area. All these models agree in predicting a gradual decline with redshift of the fraction of galaxies with a low SFR.

As far as the “Quiescent” fraction is concerned, we note that most models quantitatively agree in their prediction at all redshifts. There is a general tendency to slightly over predict the fraction of “Quiescent” galaxies, although the relatively large error bars of our sample prevent firm conclusions. As we show in more details in S09 (see also Daddi et al. 2007b), this is the result of an overall underestimate of the median SSFR of massive galaxies, which increases the number of the mildly star-forming galaxies that we detect within our selection criteria  $\dot{M}/M_* < (t_U(z))^{-1}$ . The F07 models provides a noticeable exception to this process. A main success of this model, indeed, is its capability of reproducing the Scuba counts and the large SFR associated: it is not surprising that it also predicts a large fraction of active galaxies, and hence a lower fraction of “Quiescent” ones.

Conversely, the predictions of the fraction of “Red&Dead” galaxies show a large variance at all redshifts. This reveals that the predicted fraction of galaxies with very low levels of SFR is a particularly sensitive quantity, and potentially provides a powerful way to emphasize the differences among the different models. Some models (M06, F07) under predict the fraction of “Red&Dead” galaxies at all redshifts, and in particular predict virtually no object at  $z > 2$ , contrary to what observed. The Millennium-based model agrees with the observed quantities, while the hydro model appears to over predict them.

It is beyond the scope of the present paper to discuss the origins of such differences. They are indeed difficult to ascertain, because of the complex interplay between all the physical processes involved in these models, the differences in physical process implemented - most notably regarding the AGN feedback - and their much different technical implementations. In any case, the failure of most models to match simultaneously the fraction of “Quiescent” and “Red&Dead” massive galaxies in the early Universe likely reveals that the balance between the amount of cool gas and the efficiency of star formation on the one side, and the different feedback mechanisms on the other, is still poorly understood.

**Acknowledgements.** We are grateful to Mark Dickinson, Roberto Maiolino and Pierluigi Monaco for the useful discussions. We also thank K. Nagamine for providing the output of his models. We are also in debt with the two referees for useful and prompt suggestions, that improved the presentation of the work. This work is based on observations carried out with the Very Large Telescope at the ESO Paranal Observatory under Program ID LP168.A-0485 and ID 170.A-0788 and the ESO Science Archive under Program IDs 64.O-0643, 66.A-0572, 68.A-0544, 164.O-0561, 163.N-0210, and 60.A-9120. The Millennium Simulation databases used in this paper and the web application providing online access to them were constructed as part of the activities of the German Astrophysical Virtual Observatory. This work has been partly funded by ASI, under the COFIS contract.

## References

- Abraham, R. G., Nair, P., McCarthy, P. J., et al. 2007, *ApJ*, 669, 184
- Arnouts, S., Walcher, C. J., Le Fèvre, O., et al. 2007, *A&A*, 476, 137
- Berta, S., Lonsdale, C. J., Polletta, M., et al. 2007, *A&A*, 476, 151

- Bower, R. G., Benson, A. J., Malbon, R., et al. 2006, *MNRAS*, 370, 645
- Brinchmann, J., Charlot, S., White, S. D. M., et al. 2004, *MNRAS*, 351, 1151
- Bruzual A, G. 2007, *ArXiv Astrophysics e-prints*
- Cimatti, A., Daddi, E., Cassata, P., et al. 2003, *A&A*, 412, L1
- Cimatti, A., Daddi, E., Renzini, A., et al. 2004, *Nature*, 430, 184
- Daddi, E., Alexander, D. M., Dickinson, M., et al. 2007a, *ApJ*, 670, 173
- Daddi, E., Cimatti, A., Pozzetti, L., et al. 2000, *A&A*, 361, 535
- Daddi, E., Cimatti, A., Renzini, A., et al. 2004, *ApJ*, 617, 746
- Daddi, E., Dickinson, M., Morrison, G., et al. 2007b, *ApJ*, 670, 156
- Dale, D. A. & Helou, G. 2002, *The Astrophysical Journal*, 576, 159
- Fiore, F., Grazian, A., Santini, P., et al. 2008, *ApJ*, 672, 94
- Fontana, A., Pozzetti, L., Donnarumma, I., et al. 2004, *A&A*, 424, 23
- Fontana, A., Salimbeni, S., Grazian, A., et al. 2006, *Astronomy & Astrophysics*, 459, 745
- Fontanot, F., Monaco, P., Silva, L., & Grazian, A. 2007, *MNRAS*, 382, 903
- Franceschini, A., Rodighiero, G., Cassata, P., et al. 2006, *A&A*, 453, 397
- Franx, M., Labbé, I., Rudnick, G., et al. 2003, *ApJ*, 587, L79
- Grazian, A., Fontana, A., De Santis, C., et al. 2006, *Astronomy & Astrophysics*, 449, 951
- Grazian, A., Salimbeni, S., Pentericci, L., et al. 2007, *Astronomy & Astrophysics*, 465, 393
- Hopkins, P. F., Cox, T. J., Kereš, D., & Hernquist, L. 2008, *ApJS*, 175, 390
- Kennicutt, Jr., R. C. 1998, *ARA&A*, 36, 189
- Kitzbichler, M. G. & White, S. D. M. 2007, *Royal Astronomical Society, Monthly Notices*, 376, 2
- Kriek, M., van Dokkum, P. G., Franx, M., et al. 2006, *ApJ*, 649, L71
- McCarthy, P. J. 2004, *ARA&A*, 42, 477
- Menci, N., Fontana, A., Giallongo, E., Grazian, A., & Salimbeni, S. 2006, *The Astrophysical Journal*, 647, 753
- Nagamine, K., Ostriker, J. P., Fukugita, M., & Cen, R. 2006, *ApJ*, 653, 881
- Papovich, C., Dickinson, M., & Ferguson, H. C. 2001, *ApJ*, 559, 620
- Papovich, C., Rudnick, G., Le Floc'h, E., et al. 2007, *ApJ*, 668, 45
- Polletta, M., Tajer, M., Maraschi, L., et al. 2007, *The Astrophysical Journal*, 663, 81
- Pozzetti, L. & Mannucci, F. 2000, *MNRAS*, 317, L17
- Salimbeni, S., Giallongo, E., Menci, N., et al. 2008, *A&A*, 477, 763
- Santini, P., Fontana, A., Grazian, A., et al. 2009, Submitted to *A&A*
- Saracco, P., Longhetti, M., Severgnini, P., et al. 2005, *MNRAS*, 357, L40
- van Dokkum, P. G., Förster Schreiber, N. M., Franx, M., et al. 2003, *ApJ*, 587, L83
- Wuyts, S., Labbé, I., Franx, M., et al. 2007, *ApJ*, 655, 51
- Yan, R., Newman, J. A., Faber, S. M., et al. 2006, *ApJ*, 648, 281
- Zirm, A. W., Stanford, S. A., Postman, M., et al. 2008, *ApJ*, 680, 224